Journal of Solid State Chemistry 182 (2009) 645–656

Contents lists available at ScienceDirect

Journal of Solid State Chemistry

journal homepage: www.elsevier.com/locate/jssc

Phase equilibria in systems Ce–*M*–Sb (*M* = Si, Ge, Sn) and superstructure $Ce_{12}Ge_{9-x}Sb_{23+x}$ ($x = 3.8 \pm 0.1$)

Navida Nasir [a], Andriy Grytsiv [a], Peter Rogl [a,*], Adriana Saccone [b], Gerald Giester [c]

[a] Institute of Physical Chemistry, University of Vienna, Währingerstr. 42, 1090 Wien, Austria
[b] Dipartimento di Chimica e Chimica Industriale, Università di Genova, Via Dodecaneso 31, I-16146 Genova, Italy
[c] Institut für Mineralogie und Kristallographie, Universität Wien, Althanstrasse 14, A-1090 Wien, Austria

ARTICLE INFO

Article history:
Received 7 October 2008
Received in revised form
4 December 2008
Accepted 13 December 2008
Available online 24 December 2008

Keywords:
Phase diagram
X-ray powder and single crystal diffraction

ABSTRACT

Phase relations in the ternary systems Ce–*M*–Sb (*M* = Si, Ge, Sn) in composition regions $CeSb_2$–Sb–*M* were studied by optical and electron microscopy, X-ray diffraction, and electron probe microanalysis on arc-melted alloys and specimens annealed in the temperature region from 850 to 200 °C. The results, in combination with an assessment of all literature data available, were used to construct solidus surfaces and a series of isothermal sections. No ternary compounds were found to form in the Ce–Si–Sb system whilst $Ce_{12}Ge_{9-x}Sb_{23+x}$ ($3.3 < x < 4.2$) and $CeSn_xSb_2$ ($0.1 < x < 0.8$) participate in phase equilibria in the composition region investigated. Crystallographic parameters for the ternary compound $Ce_{12}Ge_{9-x}Sb_{23+x}$ ($x = 3.8 \pm 0.1$) were determined from X-ray single crystal and powder diffraction. For the binary system Ge–Sb a eutectic was defined $L \Leftrightarrow$(Ge)+(Sb) at 591.6 °C and 22.5 at%. Ge EPMA revealed a maximal solubility of 6.3 at% Ge in (Sb) at the eutectic temperature.

1. Introduction

Following our general interest in phase equilibria in binary and ternary systems formed by rare earths (RE) with p^2 elements (Si, Ge, Sn) and/or with antimony, the ternary systems Ce–*M*–Sb were investigated as a logical continuation of our previous studies [1–4]. Literature information on ternary compounds in these systems is available from [5–10], whereas phase relations were only reported for the Ce–Sb–Ge system for which an isothermal section at 400 °C has been determined [6] revealing three ternary compounds: Ce_2GeSb_3 (super structure of $ThGe_2$-type), $Ce_5Ge_3Sb_2$ (unknown structure) and Ce_3GeSb (La_3GeIn-type). A subsequent investigation [7] of ternary rare earth germanium antimonides prepared from Sb-flux yielded the formation of isotypic compounds $RE_6Ge_{5-x}Sb_{11+x}$ (*RE* = La, Ce, Pr, Nd, Sm, Gd, Tb and Dy) crystallizing in the orthorhombic space group *Immm* ($La_6Ge_{2.8}Sb_{13.2}$ structure type). A detailed structural characterization by X-ray single crystal techniques was performed for $La_6Ge_{2.8(1)}Sb_{13.2(1)}$ and $Nd_6Ge_{4.3(1)}Sb_{11.7(1)}$, whereas for the other representatives of the $La_6Ge_{2.8}Sb_{13.2}$ structure type only lattice parameters were given [7].

Equilibrium phase diagrams Ce–Sn–Sb and Ce–Si–Sb have not been constructed so far, however, ternary compounds with composition $RESn_xSb_2$ (*Cmcm*, $LaSn_{0.75}Sb_2$ type, *RE* = La, Ce, Pr, Nd and Sm) were reported by [5,10].

With respect to the limited information on phase equilibria in the ternary systems Ce–*M*–Sb (*M* = Si, Ge, Sn), and in view of the contradiction concerning the formation of $Ce_6Ge_{5-x}Sb_{11+x}$ [7] (not mentioned by [6]) the ternary systems Ce–*M*–Sb (*M* = Si, Ge, Sn) became the subject of our studies in the region $CeSb_2$–Sb–*M* (Ge, Sn, Si). Furthermore details will be elucidated for the structures of $Ce_6Ge_{5-x}Sb_{11+x}$ (found to be a superstructure with formula $Ce_{12}Ge_{9-x}Sb_{23+x}$ in current work) and $CeSn_xSb_2$.

2. Experimental

All samples, each of a total amount of ca. 1 g, were prepared in an electric arc furnace under Ti-gettered argon with a non-consumable tungsten electrode on a water cooled copper heath. The purity of cerium was 99.5 mass%, the purity of antimony, germanium, silicon and tin was better than 99.9%. The alloys were remelted three times in order to achieve complete fusion and homogeneity. Weight losses were found to be less than 1–2 mass% and were attributed to most volatile elements Sb and Sn. Final decision on phase solubilities and extent of phases was based on electron probe micro-analyses (EPMA) data (see below). After melting, alloys were subjected to annealing in evacuated quartz tubes with subsequent quenching in water. Alloys for the systems Ce–Ge–Sb and Ce–Si–Sb were annealed at 400 (30 days) and

* Corresponding author. Fax: +43 1 4277 9524.
E-mail address: peter.franz.rogl@univie.ac.at (P. Rogl).

0022-4596/$ - see front matter © 2008 Elsevier Inc. All rights reserved.
doi:10.1016/j.jssc.2008.12.009

600 °C (14 days) and alloys for the Ce–Sn–Sb system were annealed at 200 (90 days) and 400 °C (14 days).

X-ray powder diffraction data from as-cast and annealed alloys were collected with a Guinier–Huber image plate system (Cu$K\alpha_1$ or Fe$K\alpha_1$; $8° < 2\theta < 100°$). Precise lattice parameters were calculated by least-squares fits to indexed 2θ-values employing Ge as internal standard ($a_{Ge} = 0.565791$ nm).

To determine the crystal structure of $Ce_{12}Ge_{9-x}Sb_{23+x}$, a single crystal fragment, suitable for X-ray structure determination was broken from an arc-melted sample with nominal composition $Ce_{25}Sb_{62.5}Ge_{12}$, which had been vacuum-sealed in a quartz tube and annealed for 14 days at 600 °C prior to quenching in cold water. Inspection on an AXS-GADDS texture goniometer assured high crystal quality, unit cell dimensions and Laue symmetry of the specimens prior to X-ray intensity data collection on a four-circle Nonius Kappa diffractometer equipped with a CCD area detector and employing graphite monochromated Mo$K\alpha$ radiation ($\lambda = 0.071073$ nm). Orientation matrix and unit cell parameters for an orthorhombic system were derived using the program DENZO [11]. No absorption correction was necessary because of the rather regular crystal shape and small dimensions of the investigated specimen. The structure was solved by direct methods and refined with the SHELXL-97 and SHELXS-97 programs [12].

The as cast and annealed samples were polished using standard procedures and were examined by optical metallography and scanning electron microscopy (SEM). Compositions for Ce–Si–Sb and Ce–Ge–Sb alloys were determined via EPMA on a Carl Zeiss DSM 962 equipped with a Link EDX system operated at 20 kV and 60 μA and on a Carl Zeiss EVO 40 equipped with a Pentafet Link EDX system operated at 20 kV. Binary compounds $CeSb_2$ and CeSb were used as EPMA standards. Difference between measured values and nominal compositions were found to be within 3 at%.

Isothermal reaction temperatures were derived from thermal arrests determined in a calibrated Netzsch STA 409 PG/4/G Luxx Differential Scanning Calorimeter (DSC) employing a heating rate of 5 K/min in Al_2O_3 crucibles under a stream of 6N argon. Prior to DTA the alloys were annealed at 520 °C for 5–7 days.

3. Results and discussions

3.1. Binary boundary systems

Information regarding the binary boundary systems was taken from [13] as well as from [14] on the existence of two modifications for $CeSb_2$. Crystallographic data for the relevant solid phases from literature and/or from our current work are summarized in Table 1. During our investigation we came across two conflicting situations concerning (i) the constitution of the Ge–Sb phase diagram and (ii) the crystal structure of $Ce_{12}Ge_{9-x}Sb_{23+x}$.

3.1.1. The binary phase diagram germanium–antimony

The binary Ge–Sb phase diagram as a result of our investigation is shown in Fig. 1a. It differs from the phase diagram given in [13] (compilation of data of various authors [15–19]) by two major facts: (i) eutectic composition (85.5 at% Sb after [13] and 77.5 at% Sb (this work)) and (ii) maximal solubility of Ge in Sb (no solubility after [13] and 6.3 at% Ge at 592 °C (this work)).

Six alloys Ge_xSb_{100-x} (for $x = 2.5$, 5, 10, 15, 22 and 30 at%) were investigated in the as-cast state and after anneal at 400 (45 days), 500 (7 days), 520 (7 days) and 580 °C (2 days). The binary as-cast alloys with germanium content lower than 22 at% show primary crystallization of antimony containing up to 6.3 at% Ge as well as a eutectic with composition $Ge_{22.5}Sb_{77.5}$ (Fig. 1b). Alloys with higher germanium content reveal primary grains of germanium and the eutectic at $Ge_{22.5}Sb_{77.5}$ (Fig. 1c). The solubility of Ge in primary grains of Sb increases with the overall germanium content of the samples.

In order to determine the exact solubility limits of Ge in antimony at sub-solidus temperatures the sample Ge_5Sb_{95} was annealed at 580, 500 and 400 °C for 2, 7 and 45 days, respectively. After annealing at 400 and 500 °C the sample shows grains of Sb with a maximal solubility of 2.3 and 2.8 at% Ge at 400 and 500 °C, respectively. At 580 °C the sample looks almost single phase with traces of (Ge) consistent with a maximal solubility of 4.1 at% germanium in antimony. EPMA measurements recorded from grains of the Sb-based solution are plotted in Fig. 1a in order to define the solubility range of (Sb). Compositional dependences of lattice parameters of (Sb) as shown in Fig. 1d reveal some deviation from linearity in the higher solubility range. The maximum solubility of Ge in Sb (6.3 at%) at the eutectic temperature (592 °C) is measured by EPMA on big primary grains of Sb in the alloy with 22 at% Ge and 78 at% Sb; Fig. 1b. The puzzling non-linearity of unit cell dimensions vs. composition for more than 5 at% Ge can neither be explained by tiny Ge-precipitates in the ss-(Sb) (see inset in Fig. 1b) nor by a retrograde solidus of the (Sb)-phase (lattice parameters and EPMA data of hypo- and hyper-eutectic alloys are the same!). On Ge/Sb

Table 1
Crystal structure data for relevant solid phases in the systems Ce–Sb–M (M = Ge, Si, Sn).

Phase	Pearson symbol	Space group	Structure type	Lattice parameters			Reference
				a (nm)	b (nm)	c (nm)	
(Sb)	hR2	$R\bar{3}m$	As	a = 0.45067	$\alpha = 57.11$		[13]
				0.43084	–	1.1274	[13]
(Si)	cF8	$Fd\bar{3}m$	C	0.54306	–	–	[13]
(Ge)		$Fd\bar{3}m$	C	0.56574	–	–	[13]
(Sn)	tI2	$I4_1/amd$	βSn $I4_1/amd$	0.58318	–	0.31818	[13]
CeSb	cF8	$Fm\bar{3}m$	NaCl	0.6407			[26]
α-$CeSb_2$	oC24	$Cmca$	$SmSb_2$	0.6295(6)	0.6124(6)	1.821(2)	[26]
β-$CeSb_2$	–	–	Unknown	–	–	–	[14]
SbSn	hR2	Rhomb.	Distorted, NaCl	0.4326	–	1.0693	[24]
HP-SbSn	cF8		NaCl	0.5880(4)	–	–	[21][a]
Sb_2Sn_3	cF8	$Fm\bar{3}m$	NaCl	0.615	–	–	[20]
$CeSn_3$	cP4	$Pm\bar{3}m$	$AuCu_3$	0.47214(2)	–	–	[26]
$Ce_6Ge_{5-x}Sb_{11+x}$	oI48	$Immm$	$La_6Ge_{2.8}Sb_{13.2}$	0.42972(7)	1.0740(1)	2.6791(4)	[7]
$Ce_{12}Sb_{23+x}Ge_{9-x}$	oC184	$C222$	$Ce_{12}Sb_{23+x}Ge_{9-x}$	0.86075(2)	2.15154(4)	2.68227(5)	This work; $x = 3.8 \pm 0.1$
$CeSn_xSb_2$	oC28	$Cmcm$	$LaSn_{0.75}Sb_2$	0.4228(1)	2.2868(4)	0.4478(1)	[5] for $x = 1$
				0.42370(1)	2.2834(1)	0.44594(2)	This work for $x = 0.8$

[a] Unit cell dimension given at 7.5 GPa.

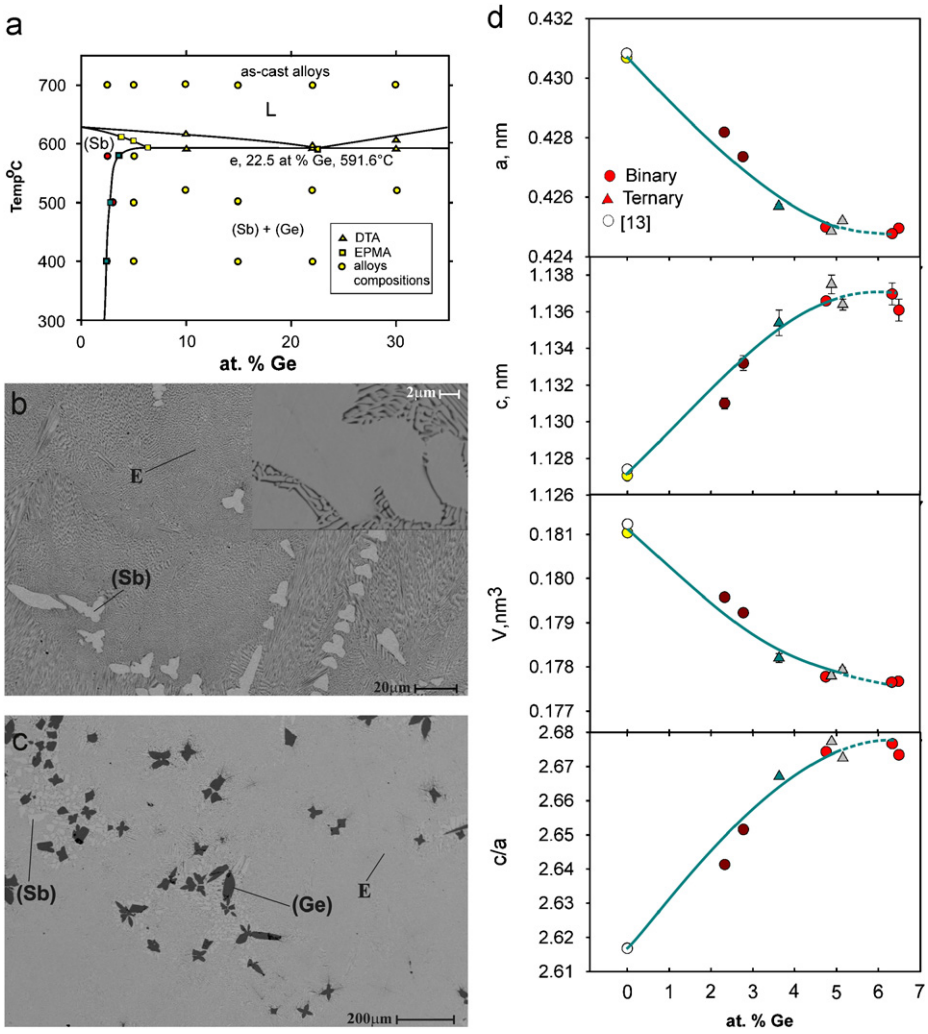

Fig. 1. (a) Binary phase diagram Ge–Sb, selected microstructures of as-cast alloys: (b) 22 at% Ge–Sb, (c) 30 at% Ge–Sb and (d) compositional dependence of lattice parameters for Sb-based solid solution.

substitution the unit cell volume decreases (Fig. 1) in line with the difference of the atomic radii of the elements. Whilst the *a*-lattice parameter in Fig. 1 decreases the *c*-parameter increases resulting in an increase of the *c*/*a* ratio from 2.617 in pure antimony to 2.677 for $Ge_{6.3}Sb_{93.6}$. It is interesting to note that Sn/Sb substitution in the related Sn–Sb system also results in a decrease of the unit cell volume but at variance to the Ge–Sb system the *c*/*a* ratio decreases with increasing tin content. Accordingly the c/a-ratio for the rhombohedral Sn–Sb phases finally reaches an ideal value of 2.4495, which corresponds to the transformation from rhombohedral to cubic unit cells. The cubic structure is reported for Sb_2Sn_3 (NaCl-type [20]) and the high-pressure form of SbSn [21].

Despite a serious disagreement with literature data on the eutectic composition in the Ge–Sb system, the temperature of the invariant (eutectic) reaction was determined by DTA at 591.6 °C in perfect agreement with literature data (592 °C, see [13]).

3.2. The crystal structure of $Ce_{12}Ge_{9-x}Sb_{23+x}$

The homogeneity region of $Ce_{12}Ge_{9-x}Sb_{23+x}$, established by EPMA, at 600 °C extends from $x = 3.3$ to $x = 4.2$. Rietveld refinements performed for the structure model reported by [7] result in an acceptable fit of X-ray powder diffraction intensities. Furthermore, single crystal X-ray data reveal tiny additional reflections (Fig. 2a) that were indexed on the basis of an orthorhombic supercell in direction *a* and *b* ($2a = 0.86075(2)$; $2b = 2.15154(4)$; $c = 2.68227(5)$ nm). It should be emphasized, that all experimentally observed intensities are indexed on the basis of the four-fold supercell. Systematic extinctions ($h+k = 2n$) consistent with Bravias *C*-type centring lead to the orthorhombic space groups *Cmmm*, *Cmm*2, *C*222 and $C2_12_12_1$. As all the space groups with higher symmetry had to be rejected because of bad *R*-values and high residual electron densities, direct methods were used to find a structure solution for space group *C*222. For the space group *C*222 (no. 21) 29 independent atom positions were found. The constitution of the unit cell is still closely related to that reported by Lam [7] (see Figs. 2b–d). Owing to close Sb18–Sb18 contacts (0.0624 nm), the occupancy of Sb18 required to be fixed at a theoretical maximum of 50% (corresponds to Sb4 in [7]). Sites *M*1, *M*2, *M*3, *M*4 were at first assumed to be occupied only by Ge. Because of the large distances (0.27–0.28 nm), which are more reasonable for Ge–Sb distances, these sites were explored as a mixture of Ge and Sb, resulting in a considerable decrease in *R*-value and residual electron density. The occupancy of the site *M*5 was fixed at a maximum of 50% because of the short interatomic distance $M5{-}M5 = 0.0839$ nm, (corresponds to *M*2 in

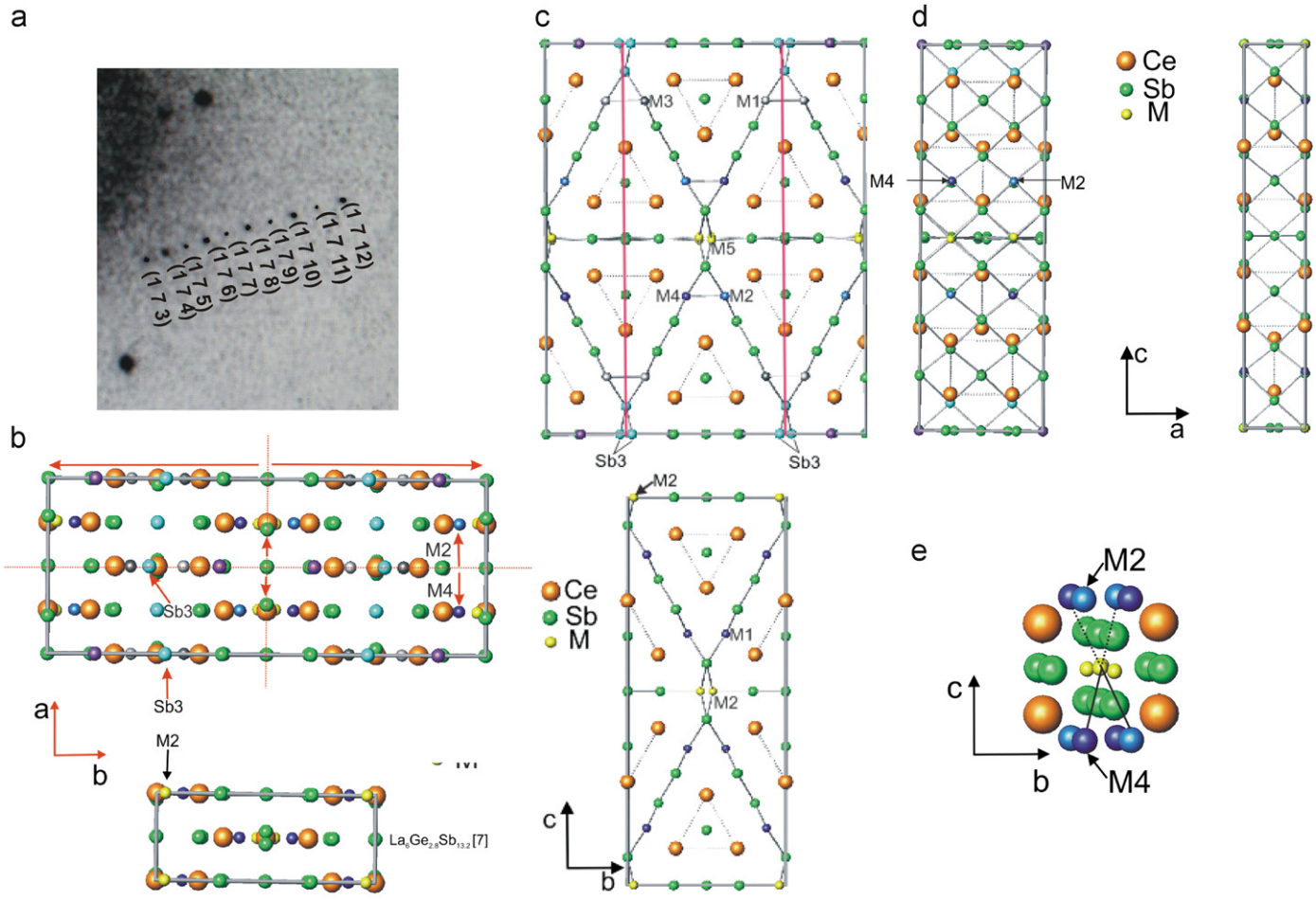

f

I2/m2/m2/m

$Ce_6Sb_{11+x}Ge_{5-x}$	Ce1: 4*i* *mm2*	Ce2: 8*l* *m..*	Sb1: 4*j* *mm2*	Sb2: 8*l* *m..*	Sb3: 4*g* *m2m*	Sb4: 4*f* *2mm*	Sb5: 4*j* *mm2*	M1: 8*l* *m..*	M2: 4*g* *m2m*
	0	0	½	0	0	*x*	½	0	0
	0	*y*	0	*y*	*y*	½	0	*y*	*y*
	z	*z*	*z*	*z*	0	0	*z*	*z*	0

t2

*I*222	Ce1: 4*i* ..2	Ce2: 8*k* 1	Sb: 4*j* ..2	Sb2: 8*k* 1	Sb3: 4*g* .2.	Sb4: 4*f* 2..	Sb5 4*j* ..2	M1: 8*k* 1	M2: 4*g* .2.
	0	*x*	0	*x*	0	x	0	*x*	0
	0	*y*	½	*y*	*y*	0	½	*y*	*y*
	z	*z*	*z*	*z*	0	1/2	*z*	*z*	0

i4
2a, 2b, c
shift of origin
(0, 1/2, 0)

*C*222 / $Ce_{12}Sb_{23+x}Ge_{9-x}$	Ce1: 8*l* Ce3: 8*l*	Ce2: 8*l* Ce4: 8*l* Ce5: 8*l* Ce6: 8*l*	Sb4: 4*i*	Sb10: 4*j*	Sb7: 4*k* Sb12: 4*k*	Sb5: 8*l* Sb8: 8*l* Sb9: 8*l* Sb15: 8*l*	Sb2: 4*g* Sb6: 4*g*	Sb14: 8*l*	Sb1[1]: 4*e*	Sb1: 4*e*	Sb18: 8*l*	Sb13: 4*i*	Sb16: 4*j*	Sb11: 4*k* Sb17: 4*k*	M1: 8*l* M2: 8*l* M3: 8*l* M5: 8*l*	Ge3[1]: 4*g*	Sb3: 4*g*	M5: 8*l*
	1	1	..2	..2	..2	1	.2.	1	2..	2..	1	..2	..2	..2	1	.2.	.2.	1
	x	*x*	0	0	¼	*x*	0	*x*	*x*	*x*	*x*	0	0	¼	*x*	*x*	0	0
	y	*y*	0	½	¼	*y*	*y*	*y*	0	0	*y*	0	½	¼	*y*	*y*	*y*	*y*
	z	*z*	*z*	*z*	*z*	*z*	0	*z*	0	0	*z*	*z*	*z*	*z*	*z*	*z*	0	0

[1] Occupancy is zero.

Fig. 2. (a) Array of single crystal X-ray diffraction spots documenting the superstructure. (b) Comparison between supercell (*C*222; $Ce_{12}Ge_{9-x}Sb_{23+x}$ ($x = 3.8 \pm 0.1$) type) and sub cell (*Immm*, $La_6Ge_{2.8}Sb_{13.2}$ type [7]). (c) Comparison of supercell ($Ce_{12}Ge_{9-x}Sb_{23+x}$ ($x = 3.8 \pm 0.1$) structure type) with [7] in direction b. (d) Comparison of super cell ($Ce_{12}Ge_{9-x}Sb_{23+x}$ ($x = 3.8 \pm 0.1$) structure type) with [7] in direction a. (e) Section from the center of unit cell showing absence of center of symmetry. *M2* is a disordered site with mixture of 33.8(4)% Ge and 66.1(4)% Sb, *M4* is a disordered site with mixture of 85.0(4)% Ge and 15.0(4)% Sb. (f) Group–subgroup scheme in the Bärnighausen formalism [22,23] for subcell $Ce_6Sb_{11+x}Ge_{5-x}$ [7] to super cell $Ce_{12}Sb_{23+x}Ge_{9-x}$.

[7]). The structure refines successfully to a low reliability factor $R_{F2} = 0.060$ at small residual electron densities less than $|5.7|\,e/Å^3$ employing anisotropic thermal displacement factors. Final refinement yields a formula $Ce_{12}Ge_{9-x}Sb_{23+x}$ ($x = 3.8 \pm 0.1$) ($Ce_{27.3}Ge_{11.8}Sb_{60.9}$ in at%) in good agreement with fairly single-phase bulk samples for which EPMA gives a composition $Ce_{26.3}Ge_{12.4}Sb_{61.3}$ (in at%). Results of the structure determination are listed in Table 2a, b and c. A table on the anisotropic atom displacement parameters (Table 2d) can be obtained from the authors on request. From Table 2b one can see that there are many

Table 2
(a) X-Ray single crystal data for $Ce_{12}Sb_{23+x}Ge_{9-x}$ ($x = 3.8 \pm 0.1$), (b) Atom parameters for $Ce_{12}Sb_{23+x}Ge_{9-x}$ ($x = 3.8 \pm 0.1$) and (c) Interatomic distances for $Ce_{12}Sb_{23+x}Ge_{9-x}$ ($x = 3.8 \pm 0.1$); standard deviations less than 0.0004 nm.

(a)

Parameter/compound	
Composition from EPMA	$Ce_{26.3}Sb_{61.3}Ge_{12.4}$
Composition from refinement	$Ce_{27.3}Sb_{60.9}Ge_{11.8}$
Formula from refinement	$Ce_{12}Sb_{23+x}Ge_{9-x}$ ($x = 3.8 \pm 0.1$).
a, *b*, *c* (nm)	0.86075(2), 2.15154(4), 2.68227(5)
μ_{abs} [mm^{-1}]	35.82
V (nm^3)	4.9674
ρ_x ($g\,cm^{-3}$)	7.117
Z	8
Radiation	SC, Mo*K*α
Data collection, 2Θ range (°);	$2 \leqslant 2\Theta \leqslant 70$; 150 sec/frame
ω-scans, scan width 2°	
Total number of frames and sets	411 and 8
Reflections in refinement	$4847 \geqslant 4\sigma(F_0)$ of 11936
Mosaicity	<0.52
Number of variables	225
$R_F^2 = \Sigma\|F_0^2 - F_c^2\|/\Sigma F_0^2$	0.06
R_{Int}	0.066
w*R*2	0.1522
GOF	1.066
Extinction (Zachariasen)	0.00006
Residual density $e^-/Å^3$;	max; min 5.71; −7.39

Standardized with program *Structure Tidy* [27]; room temperature data, redundancy >8; space group *C*222; no. 21.

(b)

Atom	Wyckoff Pos.	Occ.	*x*	*y*	*z*	U_{eq} (in $10^2\,nm^2$)
Ce1	8*l*	1.0	0.0005(2)	0.24981(4)	0.26625(5)	0.0095(2)
Ce2	8*l*	1.0	0.2506(3)	0.09708(7)	0.09457(6)	0.0103(3)
Ce3	8*l*	1.0	0.25005(10)	0.00045(9)	0.23373(5)	0.0096(2)
Ce4	8*l*	1.0	0.0001(3)	0.15297(5)	0.59461(4)	0.0102(2)
Ce5	8*l*	1.0	0.0001(3)	0.34692(5)	0.40528(4)	0.0104(2)
Ce6	8*l*	1.0	0.2495(3)	0.59678(7)	0.09473(6)	0.0105(3)
Sb1	4*e*	1.0	0.2154(2)	0	0	0.0099(3)
Sb2	4*g*	1.0	0	0.398(1)	0	0.0122(4)
Sb3	4*g*	1.0	0	0.268(2)	0	0.0250(5)
Sb4	4*i*	1.0	0	0	0.143(1)	0.0103(4)
Sb5	8*l*	1.0	0.2521(4)	0.1525(1)	0.21165(8)	0.0125(4)
Sb6	4*g*	1.0	0	0.10776(8)	0	0.0113(4)
Sb7	4*k*	1.0	1/4	1/4	0.3569(1)	0.0119(5)
Sb8	8*l*	1.0	0.5026(4)	0.09743(6)	0.28846(5)	0.0130(3)
Sb9	8*l*	1.0	0.0009(4)	0.09744(6)	0.28841(5)	0.0130(3)
Sb10	4*j*	1.0	0	1/2	0.143(1)	0.0111(4)
Sb11	4*k*	1.0	1/4	1/4	0.0717(1)	0.0203(6)
Sb12	4*k*	1.0	1/4	1/4	0.6424(1)	0.0098(5)
Sb13	4*i*	1.0	0	0	0.428(6)	0.0204(4)
Sb14	8*l*	1.0	0.2503(1)	0.14540(8)	0.49996(8)	0.0146(3)
Sb15	8*l*	1.0	0.2500(4)	0.6526(1)	0.21149(8)	0.0135(4)
Sb16	4*j*	1.0	0	1/2	0.42817(9)	0.0207(4)
Sb17	4*k*	1.0	1/4	1/4	0.928(2)	0.0195(6)
Sb18	8*l*	0.5	0.0345(3)	0.2502(1)	0.5031(1)	0.0132(6)
*M*1	8*l*	Ge: 0.544(4) Sb::0.456(4)	0.0007(5)	0.19016(8)	0.14653(7)	0.0148(4)
*M*2	8*l*	Ge: 0.338(4) Sb: 0.661(4)	0.2498(4)	0.0616(1)	0.3533(1)	0.0205(5)
*M*3	8*l*	Ge: 0.577(4) Sb: 0.423(4)	0.0013(5)	0.31187(9)	0.14764(7)	0.0173(4)
*M*4	8*l*	Ge: 0.850(4) Sb: 0.150(4)	0.2503(5)	0.0603(1)	0.6472(1)	0.0173(4)
*M*5	8*l*	Ge: 0.268(4) Sb: 0.232(4)	0.245(2)	0.019(9)	0.496(8)	0.0115(6)

(c)

Ce1	−1Sb7	0.3244		−1Sb10	0.3258		−1Sb15	0.3207	Sb18	−1Sb14	0.2913
	−1Sb12	0.3264		−1M1	0.3260		−1Sb5	0.3219		−1Sb14	0.2924
	−1Sb5	0.3326		−1Sb4	0.3262		−1Ce1	0.3332		−1Ce5	0.3231
	−1Sb9	0.3332	Sb1	−2Sb6	0.2968		−1Ce3	0.3337		−1Ce4	0.3237
	−1Sb8	0.3340		−2Sb2	0.3280		−1Ce3	0.3350		−1Sb14	0.3322
	−1Sb15	0.3342		−2Ce6	0.3299		−1Ce4	0.3358		−1Sb14	0.3332
	−1Sb5	0.3351		−2Ce2	0.3300	Sb10	−2Ce3	0.3251		−1Ce5	0.3363
	−1Sb15	0.3354		−1Sb1	0.3707		−2Ce6	0.3258		−1Ce4	0.3368
	−1*M*3	0.3451		−1Sb1	0.3299		−2Ce2	0.3262		−1Sb18	0.3711
	−1*M*1	0.3458		−1Sb2	0.3328	Sb11	−2Sb3	0.2914	*M*1−	−1*M*3	0.2619
Ce2	−1*M*3	0.3225		−1Sb6	0.3341		−2*M*1	0.3210		−1Sb15	0.2882
	−1*M*1	0.3255		−1Sb17	0.3351		−2*M*3	0.3237		−1Sb5	0.2902

Table 2. (*continued*)

	–1Sb10	0.3262		–1Sb15	0.3353		–2Ce2	0.3347		–1Sb17	0.3206
	–1Sb4	0.3268	Sb2–	–1Sb3	0.2800		–1Sb17	0.3861		–1Sb11	0.3210
	–1Sb1	0.3300		–2Sb1	0.3280	Sb12	–2Ce5	0.3258		–1Ce2	0.3255
	–1Sb2	0.3324		–2Ce2	0.3324		–2Ce4	0.3261		–1Ce6	0.3260
	–1Sb6	0.3339		–2Ce6	0.3328		–2Ce1	0.3264		–1Ce1	0.3458
	–1Sb11	0.3347	Sb3–	–1Sb2	0.2800	Sb13	–2*M*5	0.2825	*M*2–	–1*M*4	0.2624
	–1Sb5	0.3359		–2Sb11	0.2914		–2*M*5	0.2949		–1Sb9	0.2866
Ce3	–1Sb10	0.3251		–2Sb17	0.2922		–2*M*2	0.3224		–1Sb8	0.2891
	–1Sb4	0.3256		–1Sb6	0.3459		–2*M*4	0.3230		–1Sb13	0.3224
	–1Sb5	0.3327	Sb4–	–2Ce3	0.3256		–2Ce4	0.3348		–1Ce4	0.3226
	–1Sb8	0.3336		–2Ce6	0.3262		–1Sb13	0.3855		–1Sb16	0.3234
	–1Sb9	0.3337		–2Ce2	0.3268	Sb14	–1*M*5	0.2727		–1Ce5	0.3235
	–1Sb15	0.3344	Sb5–	–1*M*3	0.2830		–1Sb18	0.2913		–1Ce3	0.3469
	–1Sb9	0.3350		–1M1	0.2902		–1Sb18	0.2924		–1M5	0.3952
	–1Sb8	0.3350		–1Sb8	0.3204		–2Sb18	0.3322	*M*3–	–1*M*1	0.2619
	–1*M*4	0.3449		–1Sb9	0.3219		–2Ce5	0.3332		–1Sb5	0.2830
	–1*M*2	0.3469		–1Ce1	0.3326		–2Ce4	0.3332		–1Sb15	0.2869
Ce4	–1*M*2	0.3226		–1Ce1	0.3351		–1*M*5	0.3532		–1Ce2	0.3225
	–1Sb18	0.3237		–1Ce3	0.3327	Sb15	–1*M*3	0.2869		–1Sb11	0.3237
	–1Sb12	0.3261		–1Ce2	0.3359		–1*M*1	0.2882		–1Ce6	0.3248
	–1*M*4	0.3262	Sb6–	–2Sb1	0.2968		–1Sb8	0.3200		–1Sb17	0.3249
	–1Sb7	0.3268		–2Ce2	0.3339		–1Sb9	0.3207		–1Ce1	0.3451
	–1Sb14	0.3332		–2Ce6	0.3341		–1Ce1	0.3342	*M*4–	–1*M*2	0.2624
	–1Sb14	0.3333		–1Sb3	0.3459		–1Ce3	0.3344		–1Sb8	0.2851
	–Sb13	0.3348	Sb7–	–2Ce1	0.3244		–1Ce6	0.3353		–1Sb9	0.2881
	–Sb9	0.335		–2Ce5	0.3265		–1Ce1	0.3354		–1Sb16	0.3219
	–1Sb18	0.3368		–2Ce4	0.3268	Sb16	–2*M*5	0.2888		–1Sb13	0.3230
Ce5	–1Sb18	0.3231	Sb8–	–1*M*4	0.2851		–2*M*5	0.3009		–1Ce5	0.3252
	–1*M*2	0.3235		–1*M*2	0.2891		–2*M*4	0.3220		–1Ce4	0.3262
	–1*M*4	0.3252		–1Sb15	0.3200		–2*M*2	0.3234		–1Ce3	0.3449
	–1Sb12	0.3258		–1Sb5	0.3204		–2CE5	0.3350	*M*5–	–1Sb14	0.2727
	–1Sb7	0.3265		–1Ce3	0.3336		–1Sb16	0.3854		–1Sb13	0.2825
	–2Sb14	0.3332		–1Ce1	0.3340	Sb17	–2Sb3	0.2922		–1Sb16	0.2888
	–1Sb16	0.3350		–1Ce3	0.3351		–2*M*1	0.3206		–1Sb13	0.2949
	–1Sb8	0.3354		–1Ce5	0.3354		–2*M*3	0.3249		–1Sb16	0.3009
	–1Sb18	0.3363	Sb9–	–1*M*2	0.2866		–2Ce6	0.3351		–1Sb14	0.3532
Ce6	–1*M*3	0.3248		–1*M*4	0.2881		–1Sb11	0.3861		–1*M*2	0.3952

general positions, which are very close to special positions, e.g. Ce4 (0.0001,0.15297,0.59461) close to (0,*y*,*z*) and Ce1 (0.0005,0.24981,0.26625) close to (0,$\frac{1}{4}$,*z*) which are special positions in the centro-symmetric space groups *Cmmm* and *Cmma*. Attempts to solve the structure within the space groups *Cmmm* and *Cmma*, however, were not successful with *R*-values not less than 16% and 14% and residual electron densities as high as 27.0 and 13.0 e/Å^3, respectively. When the center of symmetry is removed (*C*222) the *R*-value immediately drops. The absence of a center of symmetry increases the degree of freedom for the disordered sites *M*2, *M*4, which are random mixtures of 34(4)%Ge and 66(4)%Sb, and 85(4)%Ge and 15%Sb, respectively (Fig. 2e). These atom sites cannot be related by an inversion center or by a mirror plane. Actually, the different electron density at these sites (*M*2 and *M*4) is responsible for the presence of the superstructure in the lattice (see Fig. 2b). Refinement of the X-ray powder diffraction profiles strictly based on this structure model was successful with an *R*-value less than 6% even without refining the positional parameters and occupancies (Fig. 3). Parameters from refinement of X-ray powder diffraction are listed in Table 6 (position parameters and occupancies are same as in Table 2b).

Figs. 2c and d show the geometrical relation in direction b and a, respectively, between the super cell (*C*222) and the sub cell (*Immm*) reported by [7]. From this comparison it is obvious that all atoms on the left side (Fig. 2b) are related by a two-fold axis (parallel c) at ($\frac{1}{2}$,$\frac{1}{2}$,0) to the atoms on the right side thereby giving rise to a doubling of the unit cell in direction b. Similarly, shifting atom Sb3 off the position (0,$\frac{1}{4}$,0) to (0,0.268,0) creates another Sb3 atom via the two-fold axis (parallel c) at ($\frac{1}{4}$,$\frac{1}{4}$,*z*). The doubling of the unit cell in the a-direction can be seen from the atoms *M*4 (34%Ge and 66%Sb) and *M*2 (85%Ge and 15%Sb). Fig. 2b explains the reason for the superstructure in both directions a and b. Construction of the unit cell is very similar to the subcell established by [7] for $La_6Ge_{2.8(1)}Sb_{13.2(1)}$. The supercell consists of Sb centered trigonal prisms Ce_6Sb. Constituents of these trigonal prisms are (i) vertexes of Ce1, 4 and 5 centered by Sb7 and Sb12, (ii) vertexes of Ce2, 3 and 6 centered by Sb4 and Sb10, which share triangular faces to form columns running along [100] as described by [7]. The columns are separated by interconnecting walls of Ge and Sb atoms. A distortion in Sb-ribbons along the *a*-axis described by [7] is also seen in the present work with the difference that two short distances, $d_{Sb2-Sb1} = 0.2968$ nm, alternate with two long distances, $d_{Sb1-Sb7} = 0.3281$ nm.

Another difference observed between the two structure types is that the disordered site *M*2 in $La_6Ge_{2.8}Sb_{13.2}$ is replaced by two different atom sites (disordered site *M*5 and Sb3) in $Ce_{12}Ge_{9-x}Sb_{23+x}$ (Fig. 2b and c).

A formal group-subgroup relation is presented in Fig. 2f in the Bärnighausen formalism [22,23]. Starting from the subcell space group *Immm* the symmetry reduction goes via a "translationengleiche" symmetry reduction of index 2 (*t*2) to the space group *I*222 followed by an isomorphic transition of index 4 (*i*4) from *I*222 to *C*222 accompanied by a shift of origin of (0,$\frac{1}{2}$,0) and a fourfold increase of the cell volume (2a,2b,c). In going from *I*222 to *C*222 Wyckoff position 4*f* splits into sites 4*e*, 4*e*, 8*l*. Occupancy of 4*f* in the subcell was fixed at 50% [7]. Accordingly after splitting the occupancy in the super cell is again fixed at 50% for the 8*l* site, the 4*e* site is fully occupied by Sb1, while the second

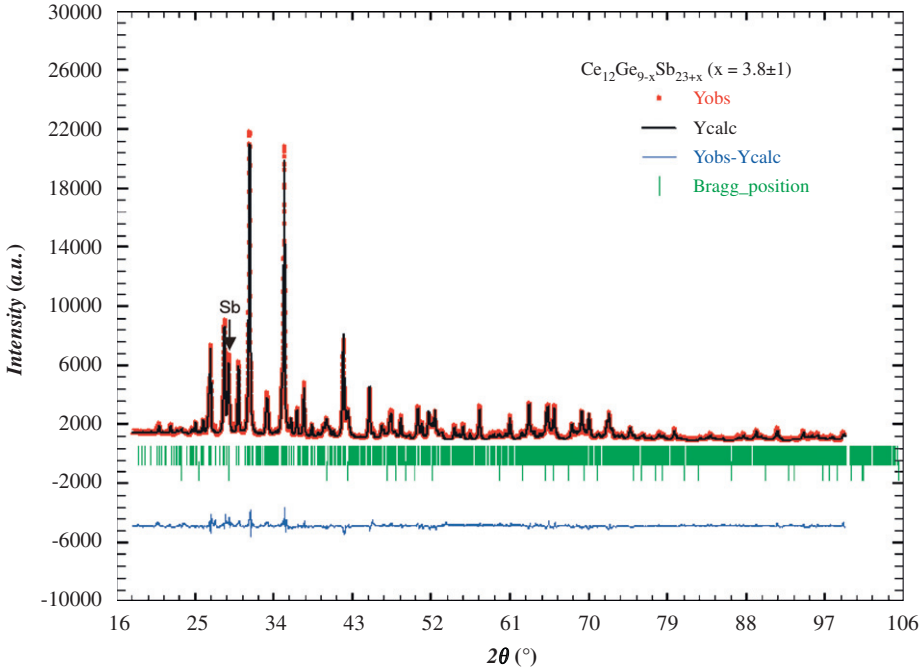

Fig. 3. X-ray Rietveld refinement for $Ce_{12}Ge_{9-x}Sb_{23+x}$ ($x = 3.8 \pm 0.1$) (nominal composition $Ce_{25}Sb_{62.5}Ge_{12.5}$).

4*e* site remains vacant. Similarly, the 4*g* site, occupied by a random mixture *M*2 (occ. 50%) in the subcell, splits into the supercell sites 4*g*, 4*g*, 8*l*. Whereas 8*l* is a disordered site *M*5 (occ. 50%), 4*g* is occupied by Sb3 but the second 4*g* site remains vacant. Thus the atom arrangement in the supercell drifts towards a more ordered arrangement although in some sites still random mixtures of Sb/Ge-atoms prevail. With respect to the fact that all experimentally observed intensities are indexed on the basis of the supercell, which simply originates from the subcell by atom/vacancy order, we may safely rule out the possibility of a structure masked by twinning.

3.3. *Phase equilibria in ternary systems Ce–M–Sb (M = Si, Ge, Sb)*

3.3.1. *Ce–Si–Sb system*

Analysis of the alloys in as-cast state and after anneal at 600 °C detected no ternary compounds in the Sb–Si–$CeSb_2$ part of the system. All diffraction peaks were indexed based on structures reported in literature for binary or unary phases revealing the phase equilibria as they are shown in Fig. 4. The solubility limits for the phases in the ternary system were determined by EPMA to be less than 0.5 at%. Microstructure of as-cast alloy $Ce_{30}Si_{35}Sb_{35}$ (Fig. 5a) shows the primary crystallization of CeSb, secondary grains of $CeSb_2$ (α) and a eutectic structure. Joint crystallization of α-$CeSb_2$ and (Si) is documented in Fig. 5b that shows the primary grains of these phases embedded in the (Sb) matrix. It has to be noted that LOM- and SEM-images of the alloys annealed at 600 °C for 30 days are very similar to those observed in as-cast state (Fig. 4): only a small coarsening of the eutectic structures was observed. In order to ensure that equilibrium conditions were reached after annealing of bulk alloys at 600 °C, powders of the samples were compacted and additionally heat-treated at 600 °C for 60 days. Subsequent X-ray characterization of the sintered samples confirms identical phase equilibria as observed in as-cast conditions and after anneal of the bulk samples at 600 °C. Data on phase composition and lattice parameters are summarized in Table 3.

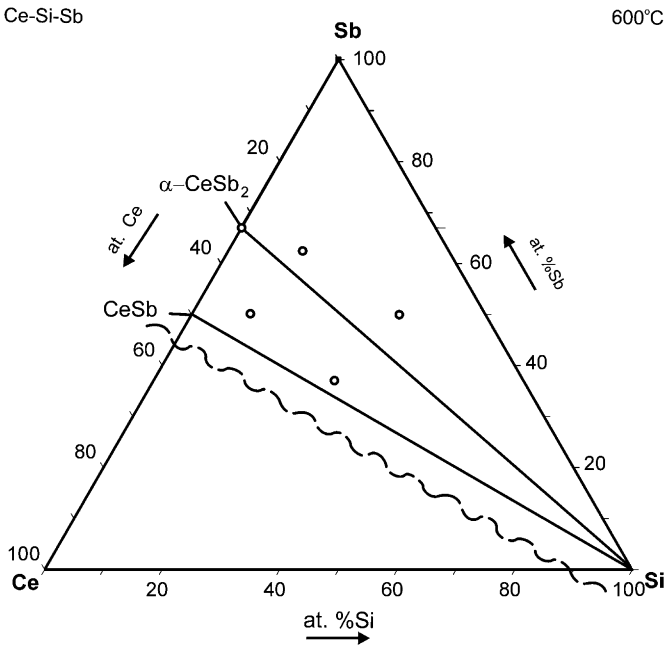

Fig. 4. Partial isothermal section of Ce-Si-Sb phase diagram at 600 °C.

3.3.2. *Ce–Ge–Sb system*

Investigation of the region CeSb–Sb–Ge reveals phase equilibria that are different from those reported by [6] for

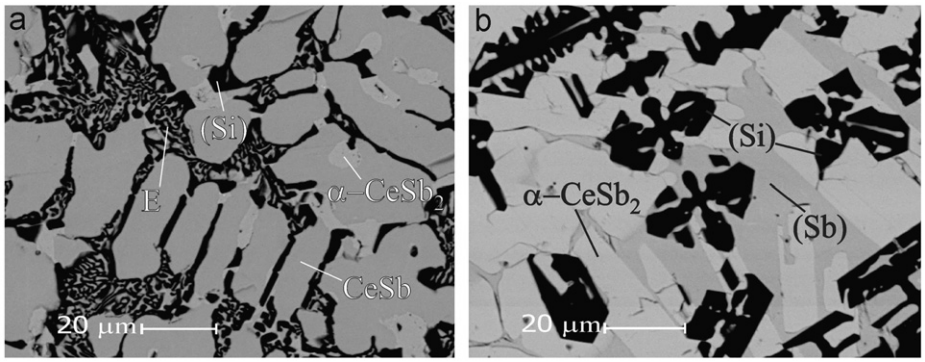

Fig. 5. Microstructure of selected Ce–Si–Sb as-cast alloys: (a) $Ce_{30}Sb_{35}Si_{35}$ and (b) $Ce_{15}Sb_{50}Si_{35}$.

Table 3
Ce-Si-Sb System (600 °C): Three-phase equilibria and lattice parameters.

Phase region T(°C)	Phase	Composition by EPMA in at%			Lattice parameters		
		Ce	Sb	Si	a (nm)	b (nm)	c (nm)
α-$CeSb_2$+(Sb)+(Si)	$CeSb_2$	31.4	68.2	0.4	0.6273(1)	0.6151(1)	1.8228(3)
	(Sb)	0.0	100	0.0	0.43085(5)	–	1.12690(2)
	(Si)	0.0	9.7	90.3	0.54303(8)	–	–
α-$CeSb_2$+CeSb+(Si)	$CeSb_2$	32.2	67.8	0.0	0.6269(3)	0.6148(3)	1.823(2)
	CeSb				0.64256(5)	–	–
	(Si)	0.0	0.6	99.4	0.54309(8)	–	–

400 °C (Fig. 6a). As-cast samples (Figs. 7a and c) were found to contain a small quantity of ternary compounds $CeSb_{2-x}Ge_x$ ($ThGe_2$ type structure [6]) and $Ce_{12}Ge_{9-x}Sb_{23+x}$ ($3.3<x<4.2$) (τ, own type structure). LOM and SEM characterization of the alloys in as-cast state and after anneal at 400 °C for 20 days yields very similar microstructures. The observation suggests that equilibrium conditions were not reached during anneal at 400 °C despite the temperature is close to solidus in the Ge–Sb binary system (592 °C, Fig. 1a). In order to ensure that samples represent equilibrium conditions, the specimens were annealed at 600 °C for 7–10 days. Selected samples were cut in parts and were additionally annealed at 520 °C for 7 days and 400 °C (30 days). Subsequent characterization of the specimens after anneal at 600, 520 and 400 °C reveals phase equilibria that significantly differ from those reported by [6]. An extended crystallization field for binary CeSb covers a significant part of the liquidus surface in the ternary system, and primary crystallization of this phase was observed in alloy $Ce_{30}Sb_{35}Ge_{35}$ (Fig. 7a). Besides of primary grains of CeSb the microstructure shows secondary crystallization of the ternary compound $CeSb_{2-x}Ge_x$ (16.1 at% Ge after EPMA) and (Ge). CeSb was also observed in small quantity in the as-cast alloy $Ce_{25}Sb_{50}Ge_{25}$ but it completely disappears after anneal at 600 °C (Fig. 7b); thus the equilibrated specimen consists of (Ge), α-$CeSb_2$ and $Ce_{12}Ge_{9-x}Sb_{23+x}$ (τ). Primary crystallization of α-$CeSb_2$ is observed in as-cast $Ce_{15}Sb_{50}Ge_{35}$ (Fig. 7c) whilst a high temperature modification (β-$CeSb_2$) was detected in both alloys $Ce_{15}Sb_{65}Ge_{20}$, and $Ce_{25}Sb_{70}Ge_5$ (Fig. 8a and c). The high-temperature modification β-$CeSb_2$ decomposes on cooling and thus the annealed alloys $Ce_{25}Sb_{70}Ge_5$ and $Ce_{25}Sb_{52}Ge_{23}$ (Fig. 7b) contain only the low-temperature form of $CeSb_2$.

Based on the character of the crystallization of the as-cast alloys, phase constituents of the annealed samples and DTA (performed on the alloys annealed at 520 °C), we constructed the solidus surface and isothermal sections at 600 and 400 °C for the Sb–$CeSb_2$–Ge part of the diagram (Fig. 6b–d and Table 4).

Samples from composition triangle (Ge)–(Sb)–τ are in liquid–solid state at 600 °C. Consequently the ternary compound (τ) was found in equilibrium with liquid that crystallizes on quenching under formation of (Sb) and a cerium-depleted eutectic (Fig. 8d). The composition of this ternary eutectic $Ce_{<0.3}Ge_{\sim 23}Sb_{\sim 77}$, as measured by EPMA on as-cast alloys (Figs. 7c, 8a and c), is very close to the binary Sb–Ge eutectic ($Ge_{22.5}Sb_{77.5}$, see Fig. 1a). Particularly, the melting point of the ternary eutectic $L=\tau$+(Ge)+(Sb) ($T_E=591\pm1$ °C) is almost identical with the binary invariant reaction $L=$(Ge)+(Sb) (591.6 °C). The temperature of 604 °C on solidus surface (Fig. 6d) corresponds to the formation of τ via an invariant reaction L+α-$CeSb_2=\tau$+(Sb). In order to determine the temperature stability range for the ternary compound τ, the alloy with composition $Ce_{25}Ge_{62.5}Sb_{12.5}$ was annealed at 400, 520, 600, 650, 700, 750, 800 and 850 °C. From XPD the existence of the ternary compound is confirmed for the temperature range from 400 to 800 °C whilst alloys quenched from 850 °C do not contain the ternary compound but instead consist of β-$CeSb_2$+(Ge)+(Sb). Due to the high vapor pressure of antimony at temperatures above 800 °C no DTA analyses were performed to determine the decomposition temperature of this ternary compound.

Phase equilibria at 400 °C were found to be the same as at subsolidus temperature (Fig. 6b). The difference only concerns the maximal solubility of Ge in Sb that decreases from 6.3 at% Ge at solidus temperatures to about 2.4 at. Ge at 400 °C.

3.3.3. *Ce–Sn–Sb system*

Ce–Sn–Sb alloys were investigated in three states: as-cast, after anneal of the bulk samples at 400 (15 days) and 200 °C (60 days).

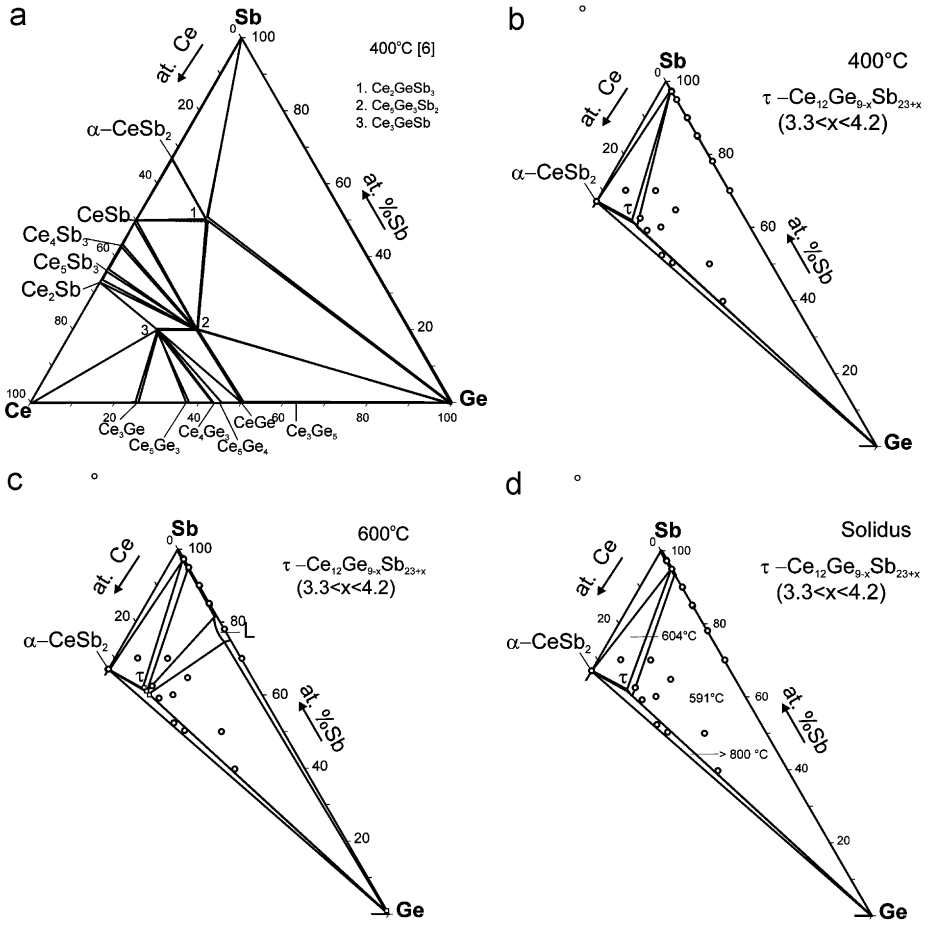

Fig. 6. Phase diagram of Ce–Ge–Sb system: (a) isothermal section at 400 °C after [6], (b) 400 °C and (c) 600 °C (this work) and (d) solidus surface (this work).

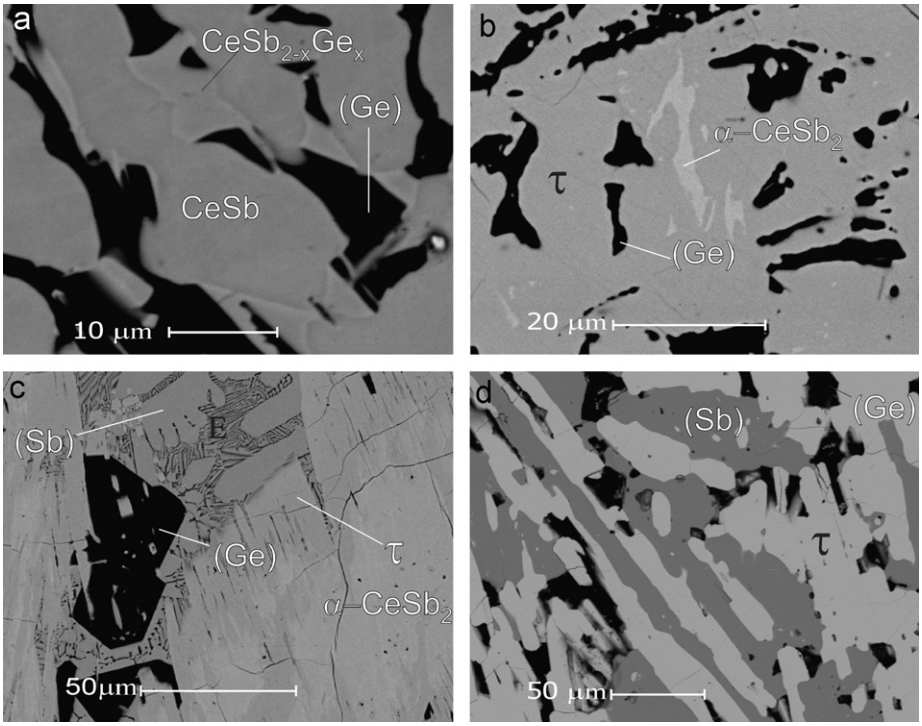

Fig. 7. Microstructure of selected Ce–Ge–Sb alloys: (a) $Ce_{30}Sb_{35}Ge_{35}$ (as-cast), (b) $Ce_{25}Sb_{52}Ge_{23}$ (600 °C), (c) $Ce_{15}Sb_{50}Ge_{35}$ (as-cast), (d) $Ce_{15}Sb_{50}Ge_{35}$ (600 °C).

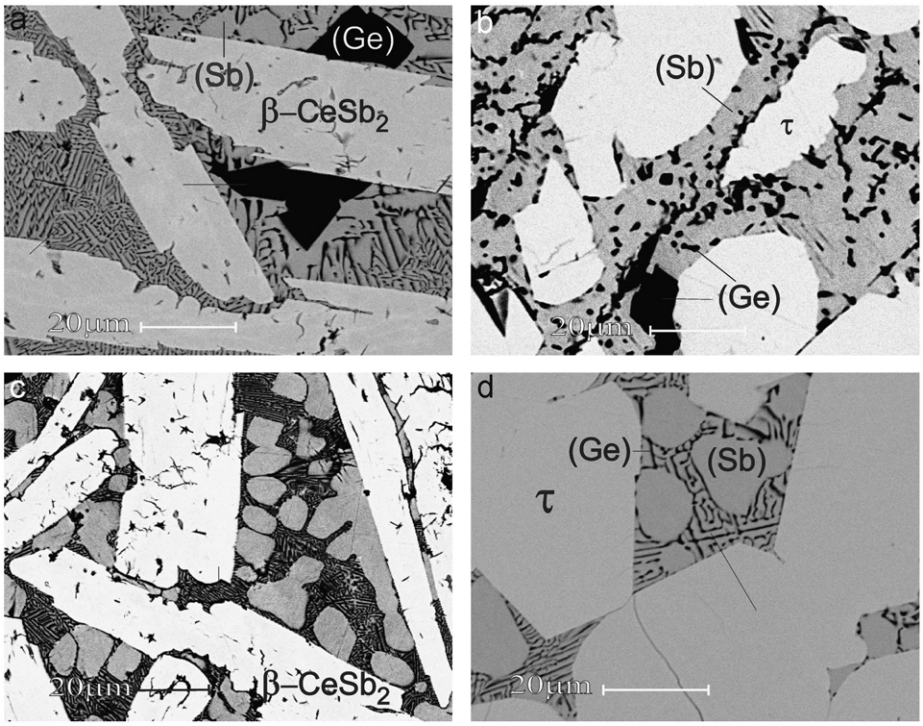

Fig. 8. Microstructure of selected Ce–Ge–Sb alloys: (a) $Ce_{15}Sb_{65}Ge_{20}$ (as-cast), (b) $Ce_{15}Sb_{65}Ge_{20}$ (600 °C), (c) $Ce_{25}Sb_{70}Ge_5$ (as-cast), (d) $Ce_{12}Sb_{62.5}Ge_{12.5}$ (600 °C).

Table 4
Ce-Ge-Sb System (solidus): Three-phase equilibria and lattice parameters.

Phase region T(°C)	Phase	Composition by EPMA in at%				Lattice parameters	
		Ce	Sb	Ge	a (nm)	b (nm)	c (nm)
τ+(Sb)+(Ge)	τ	26.1	61.9	12.0	0.85902(8)	2.1456(1)	2.6773(5)
	(Sb)	–	94.4	5.6	0.42546(6)	–	1.1368(2)
	(Ge)	–	0.8	99.2	0.56561(9)	–	–
τ+α-$CeSb_2$+(Sb)	τ	26.0	63.5	10.5	0.8530(3)	2.1632(3)	2.712(4)
	α-$CeSb_2$	31.7	68.3	0.0	0.62739(7)	0.6153(1)	1.8206(7)
	(Sb)	0.0	96.4	3.6	0.42579(3)	-	1.1362(4)
τ+α-$CeSb_2$+(Ge)	τ				0.86082(3)	2.1506(1)	2.6810(2)
	α-$CeSb_2$				0.6269(3)	0.6150(2)	1.8166(9)
	(Ge)				0.56575(4)	–	–

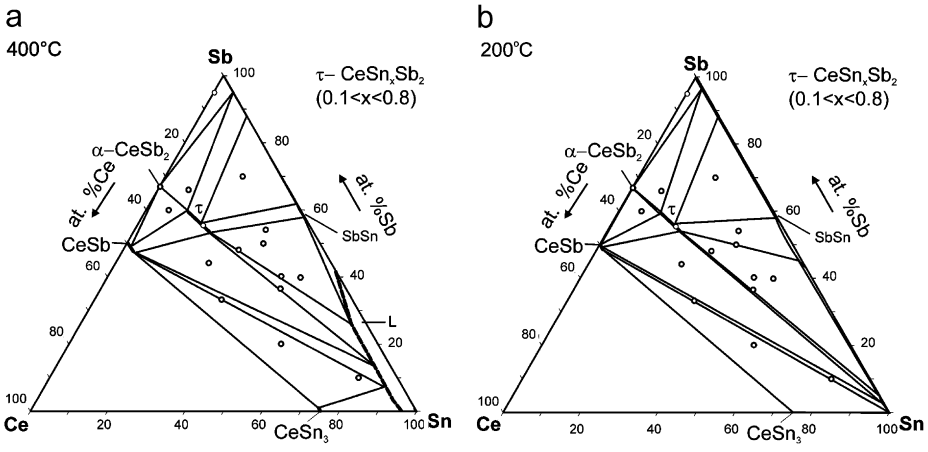

Fig. 9. Partial isothermal section of Ce–Sn–Sb phase diagram at (a) 400 °C and (b) 200 °C.

Table 5
Ce-Sn-Sb System: Three-phase equilibria and lattice parameters for alloys annealed at 400 and 200 °C.

Phase region T(°C)	Phase	Lattice parameters		
		a (nm)	b (nm)	c (nm)
400 °C				
τ+SbSn+(Sb)	τ	0.42420(4)	2.2827(2)	0.44556(6)
	SbSn	0.4324(1)	–	1.0731(5)
	(Sb)	0.42597(4)	–	1.1456(2)
τ+α-$CeSb_2$+(Sb)	τ	0.42477(5)	2.2808(2)	0.44369(3)
	α-$CeSb_2$	0.6380(1)	0.6027(9)	2.00(1)
	(Sb)	0.42732(8)	–	1.1417(2)
τ+CeSb+α-$CeSb_2$	τ	0.42373(7)	2.2833(4)	0.44483(7)
	CeSb	0.64241(5)	–	–
	α-$CeSb_2$	0.62621(1)	0.6175(2)	1.817(3)
τ+SbSn+*L*	τ	0.42301(6)	2.2867(2)	0.44768(3)
	SbSn	0.43218(5)	–	1.0690(4)
	(Sn)[a]	0.58392(3)	–	0.31819(3)
CeSb+$CeSn_3$+*L*	CeSb	0.64235(8)	–	–
	$CeSn_3$	0.47225(4)	–	–
	(Sn)[a]	0.58323(3)	–	0.31832(2)
τ+CeSb+*L*	τ	0.42238(5)	2.2852(3)	0.44826(4)
	CeSb	0.64225(3)	–	–
	(Sn)[a]	0.58367(3)	–	0.31820(3)
200 °C				
τ+SbSn+(Sb)	τ	0.0.42374(5)	2.2817(6)	0.44586(7)
	SbSn	0.4314(1)	–	1.0763(6)
	(Sb)	0.42586(5)	–	1.1458(4)
τ+α-$CeSb_2$+(Sb)	τ	0.42390(7)	2.2837(6)	0.44501(8)
	α-$CeSb_2$	0.61278(8)	0.6162(8)	1.819(4)
	(Sb)	0.42666(8)	–	1.1448(4)
τ+CeSb+α-$CeSb_2$	τ	0.42543(2)	2.2824(7)	0.4458(1)
	CeSb	0.64236(5)	–	–
	α-$CeSb_2$	0.6275(3)	0.6165(5)	1.812(4)
τ+SbSn+(Sn)	τ	0.42253(5)	2.2848(8)	0.44787(7)
	SbSn	0.43375(2)	–	1.0701(4)
	L(Sn)[a]	0.58385(5)	–	0.31807(3)
CeSb+$CeSn_3$+*L*	CeSb	0.64242(9)	–	–
	$CeSn_3$	0.4726(1)	–	–
	(Sn)[a]	0.58333(4)	–	0.31824(3)
τ+CeSb+*L*	τ	0.42257(4)	2.2851(4)	0.44814(8)
	CeSb	0.64238(5)	–	–
	(Sn)[a]	0.58396(5)	–	0.31817(5)

[a] Alloys were in solid–liquid state. (Sn) forms during crystallization from liquid.

Isothermal sections at 400 and 200 °C have been determined for the region CeSb–Sb–Sn–$CeSn_3$ and are presented in Fig. 9 (see also data in Table 5). Formation of the ternary compound $CeSn_xSb_2$ is confirmed: the phase crystallizes incongruently and coexists in equilibrium with liquid at 400 °C. Crystallographic data for $CeSn_xSb_2$ in Table 6 were obtained from Rietveld refinements. Lattice parameter data concerning the solid phases in equilibrium at 400 °C are listed in Table 5. X-rays analysis confirms the rhombohedral symmetry for SbSn (distorted NaCl [24]) instead of the cubic NaCl type [21]. Antimony and SbSn reveal very similar X-ray diffraction patterns that differ only slightly by the angular position of the diffraction maxima. In correspondence with the difference in the atomic radii of Sb and Sn the unit cell volume and c-lattice parameter decrease with increase of tin content whilst a-increases. Following this trend towards the particular c/a ratio 2.4495 will render the X-ray diffraction spectrum very similar to that of Sb_2Sn_3 with NaCl type structure. However, we neither observe this cubic structure nor we can confirm the existence of the various rhombohedral modifications of SbSn reported in [24,25].

4. Conclusions

Phase equilibria in the systems Ce–M–Sb (M = Si, Ge, Sn) were studied in the phase region $CeSb_2$–Sb–M. A maximum solubility of Ge in Sb was found to be 6.3 at% Ge at the eutectic temperature 591.6 °C with a newly defined eutectic composition 22.5 at% Ge.

No ternary compound was found in the Ce–Si–Sb system in the phase region CeSb–Si–Sb. In the Ce–Ge–Sb system a compound τ, $Ce_{12}Ge_{9-x}Sb_{23+x}$ exists in equilibrium with a homogeneity region extending from $x = 3.3$ to $x = 4.2$. From single crystal X-ray analysis $Ce_{12}Ge_{9-x}Sb_{23+x}$ was found to adopt a superstructure of the $La_6Ge_{2.8}Sb_{13.2}$ type with space group $C222$ and lattice parameters doubled in direction a (0.86075(2) nm) and b (2.15154(4) nm) while c (2.68227(5) nm) remains the same resulting in a unit cell with volume and Z four times bigger that of the $La_6Ge_{2.8}Sb_{13.2}$ type. Partial isothermal sections at 200 and 400 °C are constructed for the Ce–Sn–Sb system. $CeSn_xSb_2$ ($0.1 < x < 0.8$) ($Cmcm$, $LaSn_{0.75}Sb_2$ type) exists in equilibrium at 200 and 400 °C.

Table 6
Crystallographic data for $Ce_{12}Ge_{9-x}Sb_{23+x}$ ($(3.3 < x < 4.2)$ and $CeSn_xSb_2$ $(0.1 < x < 0.8)$.

Parameter/compound	$CeSn_xSb_2$ ($x = 0.8$)	$Ce_{12}Ge_{9-x}Sb_{23+x}$ ($3.3 < x < 4.2$)
Space group, prototype	$Cmcm$, $LaSn_{0.75}Sb_2$	$C222$, $Ce_{12}Ge_{9-x}Sb_{23+x}$ ($x = 3.8 \pm 0.1$)
Composition, EMPA at%	–	$Ce_{26.3}Sb_{61.3}Ge_{12.4}$
Composition from refinement	$Ce_{26}Sn_{21.9}Sb_{52}$	$Ce_{27.3}Sb_{60.9}Ge_{11.8}$
a; b; c (nm), Ge standard	0.42370(1)); 2.2834(1); 0.44594(2)	0.86030(4); 2.1504(3); 2.6811(7)
Reflections measured	170	1636
Θ Range	$8 \leqslant 2\Theta \leqslant 100$	$8 \leqslant 2\Theta \leqslant 100$
Number of variables	21	21
$R_F = \Sigma\lvert F_o - F_c\rvert / \Sigma F_o$	0.0511	0.0407
$R_I = \Sigma\lvert I_o - I_c\rvert / \Sigma I_o$	0.0809	0.0598
$R_{wP} = [\Sigma w_i\lvert y_{oi} - y_{ci}\rvert^2 / \Sigma w_i\lvert y_{oi}\rvert^2]^{1/2}$	0.0534	0.0472
$R_P = \Sigma\lvert y_{oi} - y_{ci}\rvert / \Sigma\lvert y_{0i}\rvert$	0.0380	0.0359
$R_e = [(N-P+C)/\Sigma w_i y_{oi}^2)]^{1/2}$	0.0182	0.0252
$\chi^2 = (R_{wP}/R_e)^2$	8.57	3.52
Atom parameters	Ce1: 4c (0,0.13876(5),1/4); $B_{iso} = 1.75$ $M1$: 8f (0, 0.01531(2), 0.644(1)); occ. = 0.184(2) Sn; $B_{iso} = 1.16$ $M2$: 4c(0,0.00833(4),1/4); occ. = 0.155(1) Sn; $B_{iso} = 1.06$ $M3$: occ = 0.315(1) Sn; 4a(0,0,0); $B_{iso} = 1.36$ 4Sb1 in 4c(0, 0.75123(6), 1/4); $B_{iso} = 1.97$ 4Sb2 in 4c(0, 0.40763(6), 1/4); $B_{iso} = 1.89$	Fixed after single crystal refinement (Table 2a) Ce; B_{iso} = 0.224 Sb and M; B_{iso} = 0.763

X-ray powder diffraction room temperature data, image plate data, Cu$K\alpha_1$ radiation; structure standardized with program *Structure Tidy* [23] (B_{iso} is given in 10^2 nm^2).

Acknowledgments

This work was supported by the Higher Education Commission of Pakistan (HEC) under the scholarship scheme "PhD in Natural & Basic Sciences from Austria".

Appendix A. Supplementary material

Supplementary data associated with this article can be found in the online version at doi:10.1016/j.jssc.2008.12.009.

References

[1] A. Grytsiv, D. Kaczorowski, A. Leithe-Jasper, P. Rogl, M. Potel, H. Noël, A.P. Pikul, T. Velikanova, J. Solid State Chem. 165 (2002) 178.
[2] A. Grytsiv, D. Kaczorowski, A. Leithe-Jasper, V.H. Tran, A. Pikul, P. Rogl, M. Potel, H. Noël, M. Bohn, T. Velikanova, J. Solid State Chem. 163 (2002) 178.
[3] A. Grytsiv, P. Rogl, S. Berger, C. Paul, H. Michor, E. Bauer, G. Hilscher, C. Godart, P. Knoll, M. Musso, W. Lottermoser, A. Saccone, R. Ferro, T. Roisnel, H. Noel, J. Phys. Condens. Matter 14 (2002) 7071.
[4] A. Grytsiv, E. Bauer, St. Berger, G. Hilscher, H. Michor, Ch. Paul, P. Rogl, A. Daoud-Aladine, L. Keller, T. Roisnel, H. Noel, J. Phys. Condens. Matter 15 (2003) 3053.
[5] M.J. Ferguson, R.W. Hushagen, A. Mar, Inorg. Chem. 35 (1996) 4505.
[6] A.O. Stetskiv, V.V. Pavlyuk, O.I. Bodak, Pol. J. Chem. 72 (1998) 956.
[7] R. Lam, R. McDonald, A. Mar, Inorg. Chem. 40 (2001) 952.
[8] L. Deakin, R. Lam, A. Mar, Inorg. Chem. 40 (2001) 960.
[9] A.M. Mills, R. Lam, M.J. Ferguson, L. Deakin, A. Mar, Coord. Chem. Rev. 207–222 (2002) 233.
[10] L. Nore′n, R.L. Withers, F.J. Brink, J. Solid State Chem. 178 (2005) 2133.
[11] Nonius Kappa CCD Program Package COLLECT, DENZO, SCALEPACK, SORTAV, Nonius Delft, The Netherlands, 1998.
[12] G.M. Sheldrick, SHELXL-97, Program for Crystal Structure Refinement, University of Göttingen, Germany, 1997 (Windows version by McArdle, National University of Ireland, Galway).
[13] T.B. Massalski, Binary Alloy Phase Diagrams, second ed., ASM International, Materials Park, OH, 1990.
[14] V.D. Abulkhaev, Russ. J. Inorg. Chem. 42 (1997) 283.
[15] V.K. Ruttewit, G. Masing, Z. Metallkd. 32 (1940) 52.
[16] B.G. Zhurkin, V.S. Zemskov, D.A. Petrov, A.D. Suchkov, Izv. Akad. Nauk SSSR Otd. Tekh. Nauk Met. Topl. 5 (1959) 86.
[17] V.B. Predel, D.W. Stein, Z. Metallkd. 61 (1970) 909.
[18] S. Bordas, M.T. Clavaguera-Mora, B. Legendre, C. Hancheng, Thermochim. Acta. 107 (1986) 239.
[19] R.W. Olesinski, G.J. Abbaschian, Bull. Alloy Phase Diagrams 7 (1986) 219.
[20] W.P. Allen, J.H. Perepezko, Sci. Metall. Mater. 24 (1990) 2215.
[21] T.N. Kolobyanina, S.S. Kabalkina, L.F. Vereshchagin, M.F. Kachan, V.G. Losev, High Temp. High Pressure 4 (1972) 207.
[22] H. Bärnighausen, Commun. Math. 9 (1980) 139.
[23] H. Bärnighausen, U. Müller, Symmetriebeziehungen Zwischen den Raumgruppen als Hilfsmittel zur Straffen Darstellung von Strukturzusammenhängen in der Kristallchemie, University of Karlsruhe and University of GH Kassel, 1996.
[24] V. Vassiliev, M. Lelaurain, J. Hertz, J. Alloys Compd. 247 (1997) 223.
[25] V. Vassiliev, Y. Feutelais, M. Sghaier, B. Legendre, J. Alloys Compd. 314 (2001) 198.
[26] P. Villars, L.D. Calvert, Pearson's Handbook of Crystallographic Data for Intermetallic Phases, second ed., ASM International, Materials Park, OH, 1991.
[27] E. Parthé, L. Gelato, B. Chabot, M. Penzo, K. Cenzual, R. Gladyshevskii, TYPIX Standardized Data and Crystal Chemical Characterization of Inorganic Structure Types, Springer, Berlin, Heidelberg, 1994.